Peer-reviewed version available at Sensors 2017, 17, 1496; doi:10.3390/s17071496

Article

A Novel Range Compression Algorithm for The Resolution Enhancement in GNSS-SAR

Yu Zheng *, Yang Yang and Wu Chen

Department of Land Surveying and Geo-informatics, The Hong Kong Polytechnic University, Hong Kong, China; yyang1018@gmail.com (Y.Y.); wu.chen@polyu.edu.hk (W.C.)

* Correspondence: yuzheng175@gmail.com; Tel.: +852-5309-1110

Abstract: Passive Global Navigation Satellite System (GNSS)-based Synthetic Aperture Radar (SAR), known as GNSS-SAR, is a new passive radar imaging system. However, compared with conventional SAR, range resolution of GNSS-SAR is significantly lower. To improve range resolution of GNSS-SAR is an interested topic for investigation. In this paper, a novel range compression algorithm for enhancing range resolutions of GNSS-SAR is proposed. In the proposed scheme, at first, range compression is conducted by correlating the received reflected GNSS signal of intermediate frequency (IF) with the synchronized direct baseband GNSS signal in range domain. Then spectrum equalization is applied to the compressed results to suppress side lobes. Both theoretical analysis and simulation results have demonstrated that significant range resolution improvement in GNSS-SAR can be obtained by the proposed range compression algorithm, compared to the conventional range compression algorithm.

Keywords: GNSS-SAR; global navigation satellite system; synthetic aperture radar; range compression; range resolution

1. Introduction

Passive GNSS (Global Navigation Satellite System)-based SAR (Synthetic Aperture Radar), known as GNSS-SAR, is a developing synthetic aperture radar (SAR) technique for remote sensing in recent years [1,2]. Unlike conventional SAR techniques, GNSS-SAR is a passive SAR receiver which uses the signals from Global Navigation Satellite System (GNSS) such as GPS, Galileo, GLONASS or Beidou as transmission of opportunity. Due to the fact that there is no need to construct SAR transmitter, GNSS-SAR has a higher flexibility together with lower expenses than conventional SAR under various applications. However low range resolution is one of the main problems that affects the current development of GNSS-SAR [1,2,13,14,16].

With the conventional GNSS-SAR imaging algorithm which includes both range and azimuth compression, range resolution is determined by signals bandwidth and bi-static angle for sensing while azimuth resolution is determined by Doppler frequency shift[1–12,14,15,17]. But in a numbers of typical literature such as [1–12,14,15,17], the system is considered as quasi-monostatic case, which means the bi-static angle can be regarded as zero. Thus the range resolution is merely determined by signal bandwidth among these works. Concerning the value of range resolution, it is proportional to the reciprocal of doubled signal bandwidth value, and for GNSS signals, the bandwidth value is equal to the Pseudo-Random Noise (PRN) code chip rate[1,2]. Because the chip rate of GPS C/A code, P code and GLONASS P code are 1.023MHz, 10.023MHz, and 5.11MHz respectively, the range resolutions can be obtained at the levels 150 m, 15 m and 30 m, respectively; for full band Galileo E5 signal, the PRN code chip rate is 51.150MHz, thus the range resolution is achieved at 3 meters level [1–12,14,15,17]. Looking at the azimuth resolution of GNSS-SAR, the level less than 1 meter can be achieved [1,2]. Compared with traditional SAR [18–20], the range resolution of GNSS-SAR is significantly lower. To improve the range resolution, various methods have correspondingly been proposed, such as the use of multi-statistic image processing and feature extraction of scene center [13,14] and [16].

However, a shortcoming of the approaches [13,14,16] is that multi-statistic image processing method is time consuming as they are applied after generating multiple full GNSS-SAR images.

The main contribution in this paper is to propose a new range compression algorithm for GNSS-SAR signal processing to improve range compressed resolution. In the proposed algorithm, the received intermediate frequency (IF) reflected GNSS signal is correlated with the synchronized direct baseband GNSS signal at range domain for each azimuth bin for range compression. Then spectrum equalization [11] is applied to suppress side lobes of the compressed result to enhance range resolution.

The rest of the paper is organized as follows. Resolution of the conventional range compression algorithm is analyzed in section 2. Resolution of the proposed range compression algorithm is analyzed in section 3. The simulation tests are provided in section 4. Section 5 discusses the future development of this research and Section 6 provides conclusions of the paper.

2. Resolution of The Conventional Range Compression Algorithm

Based on the analysis in [1–4,9–12,14,16], the overall view of the conventional range compression algorithm at GNSS-SAR receiver can be illustrated as Figure 1.

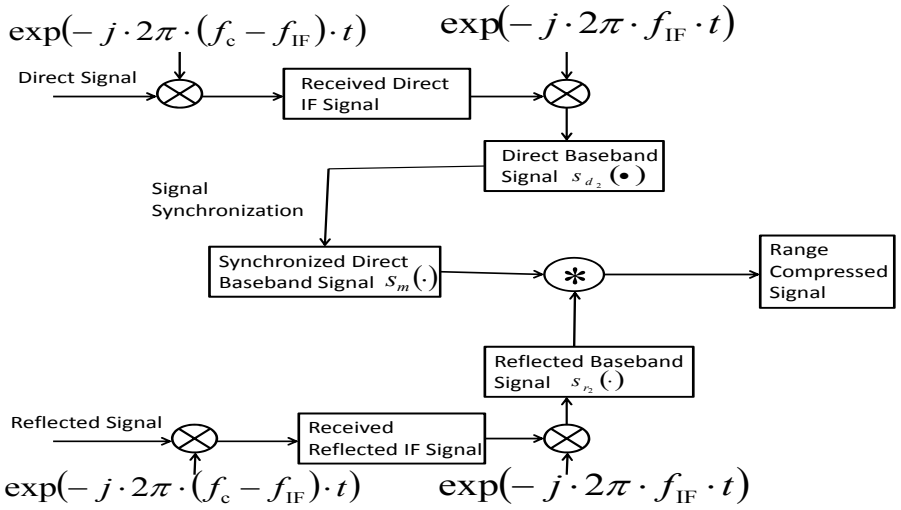

Figure 1. The conventional range compression algorithm.

In Figure 1, under the conventional range compression algorithm, both direct and reflected signals are quadrature converted to IF (Intermediate Frequency) band by multiplying the component $\exp(-j2\pi\cdot(f_c - f_{IF})\cdot t)$ at first, where f_c denotes the transmission frequency, f_{IF} denotes the intermediate frequency (IF) of the employed GNSS receiver, $\otimes$ denotes the multiplication and $\circledast$ denotes the correlation.

The received IF signals (both direct and reflected signal) are further down converted to baseband by multiplying the component $\exp(-j2\pi\cdot f_{IF}\cdot t)$. The down converted baseband direct signal can then be expressed as

$$\begin{aligned} s_{d_2}(t,u) &= A_d(t,u)\,C[t-\tau(u)]\,D[t-\tau(u)] \\ &\quad\times\exp(j(2\pi f_d\cdot t+\phi_d(u))) \\ &\quad+n_d(t,u) \end{aligned} \tag{1}$$

and reflected baseband signal can be expressed as

$$\begin{aligned} s_{r_2}(t,u) &= A_r(t,u)\, C\left[t-\tau(u)-\tau_R(u)\right] \\ &\times D\left[t-\tau(u)-\tau_R(u)\right] \\ &\times \exp\left(j\left(2\pi f_d \cdot t+\phi_r(u)\right)\right) \\ &+ n_r(t,u). \end{aligned} \tag{2}$$

where A_d and A_r denotes magnitudes of the direct and reflected signals respectively; $C(\cdot)$ denotes PRN code; $D(\cdot)$ denotes the navigation bits; t denotes the range domain; u denotes the azimuth domain; τ denotes the received direct signal delay relative to the transmitted signal; τ_R denotes the received reflected signal delay relative to the direct signal; f_d denotes Doppler frequency; ϕ_d denotes direct signal phase, and ϕ_r denotes reflected signal phase, which can be regarded as constant values within each range domain; j denotes the symbol of complex number; n_d denotes the background noise at direct channel and n_r denotes the background noise at reflected channel.

Thereafter signal synchronization based on received direct IF signal as (1) is performed, and the synchronized direct baseband signal is severed as imaging matched filter, which can be modeled as follows

$$s_m(t,u) = C\left[t-\tau(u)\right] D\left[t-\tau(u)\right] \times \exp\left(j2\pi f_d \cdot t\right). \tag{3}$$

Range compression is conducted through correlating baseband reflected signal s_{r_2} with imaging matched filter s_m at range domain, which result with respect to the noise absence term can be expressed as follows.

$$\begin{aligned} &s_{r_2} \circledast s_m^* \\ &\quad = A_r \cdot \Lambda\left(t-\tau(u)-\tau_R(u)\right) \times \exp\left(j\phi_r(u)\right) \end{aligned} \tag{4}$$

where $\Lambda(\cdot)$ indicates triangle function and its duration is determined by PRN code chip rate of GNSS signal; $*$ denotes the conjugate. In (4), because s_{r_2} and s_m are with the same frequency f_d, the frequency component after performing range correlation for the compression is canceled. Assuming the chip rate of PRN code $C(\cdot)$ is B, then the half pulse duration of the triangle function $\Lambda(\cdot)$ is derived as $\frac{1}{2B}$. Because the terms A_r and $\exp\left(j\phi_r(u)\right)$ are constants with respect to t, the duration of (4) will be determined by the term $\Lambda(\cdot)$. Thus the attainable range resolution with respect to pulse duration can be expressed as [1–4,6–11,14,17]

$$\delta_{R_1} = \frac{c}{2 \cdot \cos(\beta/2) \cdot B} \tag{5}$$

where c denotes transmission velocity of GNSS signal, β represents bi-static angle and δ_{R_1} represents the achievable range resolution by the conventional algorithm. According to (5), it can be seen that for the conventional range compression algorithm in GNSS-SAR, if bi-static angle β is fixed, the range resolution improvement can only be accomplished by employing GNSS signals with a higher PRN code chip rate $C(\cdot)$.

3. Resolution of The Proposed Range Compression Algorithm

However according to [21], we can derive that for quadrature modulated signals of $\exp(j(\cdot))$ shape, if the two signals for performing correlation have the same basedband components shaped as rectangular function but different frequencies, compared the case with the same frequencies, pulse duration of the correlated result will be shortened in the main lobe. Inspired by this, to develop a universal scheme for improving range resolution among GNSS-SAR, a new range compression algorithm is proposed, which is modeled in Figure. 2.

In Figure 2, the signals (both direct and reflected) are converted to IF band at front end GNSS receiver as well. But comparing with the conventional range compression algorithm, the proposed

Preprints (www.preprints.org) | NOT PEER-REVIEWED | Posted: 23 March 2017 doi:10.20944/preprints201703.0179.v1

Peer-reviewed version available at Sensors 2017, 17, 1496; doi:10.3390/s17071496

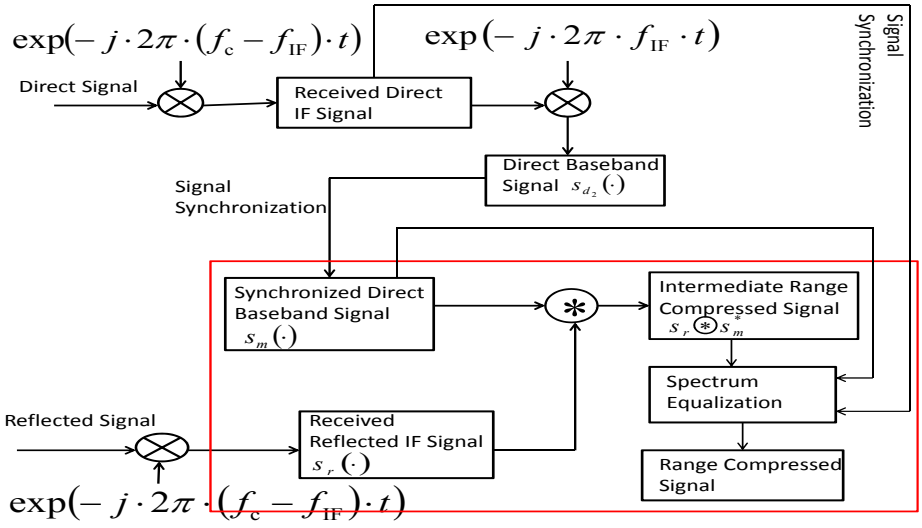

Figure 2. The proposed range compression algorithm.

new algorithm directly uses the received reflected IF GNSS signal to correlate with the synchronized direct baseband signal s_m at range domain for performing range compression, where the reflected IF GNSS signal $s_r(\cdot)$ is given as follows

$$\begin{aligned} s_r(t,u) &= A_r(t,u)\, C[t-\tau(u)-\tau_R(u)] \\ &\times D[t-\tau(u)-\tau_R(u)] \\ &\times \exp(j(2\pi(f_{\mathrm{IF}}+f_d)\cdot t+\phi_r(u))) \\ &+ n_r(t,u). \end{aligned} \tag{6}$$

And the intermediate range compressed result can be expressed as follows

$$\begin{aligned} & s_r \circledast s_m^* \\ &= A_r \cdot \Lambda(t-\tau(u)-\tau_R(u)) \\ &\times \exp(j(2\pi f_{\mathrm{IF}}\cdot t+\phi_r(u))). \end{aligned} \tag{7}$$

Based on the intermediate range compressed result (7), to suppress the compressed side lobes, spectrum equalization [11] is performed. Concerning applying spectrum equalization technique in this paper, the detailed procedure in the module 'Spectrum Equalization' in Figure 2 can be further presented as Figure 3.

As we can see that in Figure 3, Fourier transform of intermediate range compressed signal as (7) is conducted. The transformed result is expressed as follows

$$\begin{aligned} & \mathcal{F}[s_r \circledast s_m^*] \\ &= \int_0^{T-1} A_r \cdot \Lambda(t-\tau(u)-\tau_R(u)) \\ &\quad \times \exp(j(2\pi f_{\mathrm{IF}}\cdot t+\phi_r(u))) \\ &\quad \times \exp(-j2\pi\omega\cdot t)\, dt \\ &= A_r \cdot \exp(j\phi_r(u)) \\ &\quad \times \mathrm{sinc}^2(2\pi(f_{\mathrm{IF}}-\omega)) \end{aligned} \tag{8}$$

where T denotes one GNSS PRN code period; ω denotes the frequency range of the triangle function $\Lambda(\cdot)$ in (7) with an interval of $[-B, B]$. Meanwhile spectrum equalization window is designed, which is based on the reciprocal of the spectrum with respect to the correlation between the synchronized

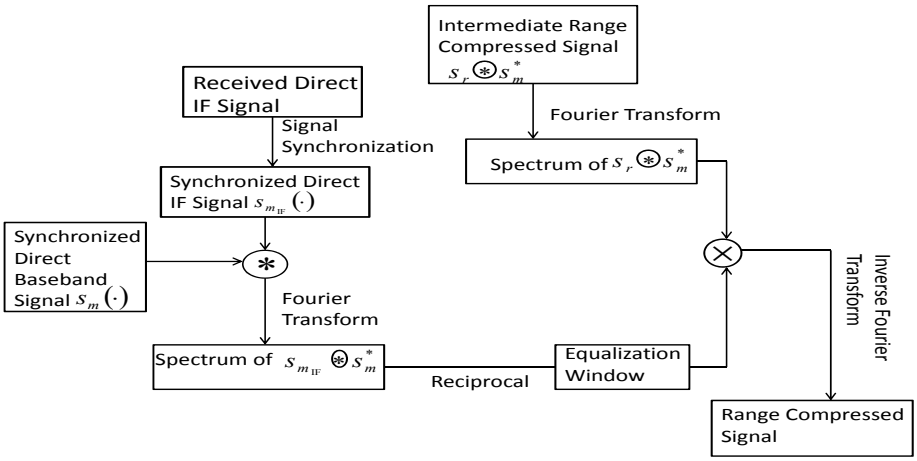

Figure 3. The proposed range compression algorithm.

direct IF signal $s_{m_{\mathrm{IF}}}$ and the synchronized direct baseband signal s_m. In Figure 3, the synchronized direct IF signal is given as follows

$$\begin{aligned} s_{m_{\mathrm{IF}}}(t,u) &= C\left[t-\tau(u)\right] D\left[t-\tau(u)\right] \\ &\quad \times \exp\left(j\left(2\pi f_{\mathrm{IF}} + f_d\right)\cdot t\right) \end{aligned} \tag{9}$$

the correlated result between $s_{m_{\mathrm{IF}}}$ and s_m is given as

$$\begin{aligned} & s_{m_{\mathrm{IF}}} \circledast s_m^* \\ &= \Lambda\left(t-\tau(u)\right) \times \exp\left(j2\pi f_{\mathrm{IF}}\cdot t\right) \end{aligned} \tag{10}$$

and the spectrum of the correlated result is the Fourier transform of (10), which can be expressed as

$$\mathcal{F}\left[s_{m_{\mathrm{IF}}} \circledast s_m^*\right] = \mathrm{sinc}^2\left(2\pi\left(f_{\mathrm{IF}}-\omega\right)\right). \tag{11}$$

Then the equalization window is designed as follows

$$W = \begin{cases} \frac{1}{\mathcal{F}\left[s_{m_{\mathrm{IF}}} \circledast s_m^*\right]} = \frac{1}{\mathrm{sinc}^2\left(2\pi\left(f_{\mathrm{IF}}-\omega\right)\right)}, & \text{when } \omega \epsilon \left[-B, B\right] \\ 0, & \text{Otherwise} \end{cases}. \tag{12}$$

The key step of spectrum equalization is performed as follows

$$\begin{aligned} & \mathcal{F}\left[s_r \circledast s_m^*\right] \times W \\ &= \begin{cases} A_r \cdot \exp\left(j\phi_r(u)\right), & \text{when frequency } \epsilon \left[f_{\mathrm{IF}}-B, f_{\mathrm{IF}}+B\right] \\ 0, & \text{Otherwise} \end{cases}. \end{aligned} \tag{13}$$

The equalized result is a rectangular function at frequency domain, where the rising edge appears at the frequency $f_{\mathrm{IF}} - B$ and the falling edge appears at the frequency $f_{\mathrm{IF}} + B$. And due to the fact that spectrum equalization is conducted at frequency domain, side lobes of the reflected signals at different range positions can be suppressed simultaneously.

To obtain the final range compressed signal, Inverse Fourier transform based on the spectrum equalized result shown in (13) is conducted. To extract the sharper pulse duration component, the

Peer-reviewed version available at Sensors 2017, 17, 1496; doi:10.3390/s17071496

lower frequency component $f_{\mathrm{IF}} - B$ is filtered out. The final range compressed signal of Figure 2 and Figure 3 is expressed as follows

$$\begin{aligned}&\mathcal{F}^{-1}\left\{\mathcal{F}\left[s_r \circledast s_m^*\right] \times W\right\} \\ &\quad = A_r \cdot \exp\left(j\phi_r\left(u\right)\right) \cdot \left(f_{\mathrm{IF}} + B\right) \\ &\quad \times \mathrm{sinc}\left[2\pi \cdot \left(f_{\mathrm{IF}} + B\right) \cdot \left(t - \tau\left(u\right) - \tau_R\left(u\right)\right)\right].\end{aligned} \tag{14}$$

In (14), the pulse duration is determined by the component $f_{\mathrm{IF}} + B$ of the $\mathrm{sinc}\left(\cdot\right)$ function term, and can be derived as $\frac{1}{f_{\mathrm{IF}}+B}$. Thus the attainable range resolution with regard to pulse duration is expressed as

$$\delta_{R_2} = \frac{c}{2 \cdot \cos\left(\beta/2\right) \cdot \left(f_{\mathrm{IF}} + B\right)} \tag{15}$$

where δ_{R_2} denotes the range resolution obtained by the proposed algorithm. It can be seen that (15) is $\frac{1}{1+f_{\mathrm{IF}}/B}$ times superior than (5) provided by conventional range compression algorithm. Meanwhile, from (14), we can see that the reflected magnitude and phase information are still preserved.

However GNSS receivers have their certain sampling frequencies, which should be considered when determine the IF value for performing range compression. Denoting the sampling frequency of GNSS receiver as f_s, according to sampling theory [22], the condition $f_{\mathrm{IF}} + B \leq \frac{1}{2} f_s$ should be satisfied. And to make the proposed algorithm because effective, the condition $f_{\mathrm{IF}} + B > B$ should be satisfied at the same time as well. Therefore, all in all, the determination of f_{IF} value should satisfy the following constraint

$$0 < f_{\mathrm{IF}} \leq \frac{1}{2} f_s - B. \tag{16}$$

Finally, azimuth compression is conducted for forming the full GNSS-SAR image based on (14) with different phase value $\phi_r\left(u\right)$ in azimuth domain.

4. The Simulation Experiment

To test the proposed algorithm for enhancing range resolution, simulations of the GNSS-SAR based on the standard GPS C/A code signal receiver configuration of ground moving mode is carried out in this section as examples. Since GPS receiver works in ground moving mode, the field of version (FOV) is mostly in horizontal, which can be considered as quasi-monostatic, the bi-static angle β can be considered as zero [2]. Thus range resolutions of the conventional algorithm and the proposed algorithm are expressed as

$$\delta'_{R_1} = \frac{c}{2B} \tag{17}$$

and

$$\delta'_{R_2} = \frac{c}{2 \cdot \left(f_{\mathrm{IF}} + B\right)} \tag{18}$$

respectively. The parameter values of the standard GPS C/A code receiver is given in Table 1.

Table 1. The parameter values of the standard GPS receiver configuration based GNSS-SAR

Parameters	Values
Supported signals type	GPS C/A code signal
PRN code chip rate B	1.023×10^6Hz
Signal transmission frequency f_c	1575.42MHz (L1 band)
Signal transmission speed c	3×10^8m/s
Number of samples in each code period	16368 samples
Sampling frequency	1.6368×10^7Hz

Based on the sampling frequency value in Table 1 and the constraint (16), two different IF frequencies $f_{\mathrm{IF}_1} = 2.092 \times 10^6$Hz and $f_{\mathrm{IF}_2} = 5.115 \times 10^6$Hz are employed in the simulation tests. Theoretically the range resolution for the conventional algorithm can be achieved at $\frac{c}{2B} = \frac{3\times10^8}{2\times1.023\times10^6} \approx 150$ m, while with the proposed algorithm in this paper, the resolution can improved to $\frac{c}{2\cdot(f_{\mathrm{IF}}+B)} = \frac{3\times10^8}{2\times(2.092\times10^6+1.023\times10^6)} \approx 50$ m and $\frac{c}{2\cdot(f_{\mathrm{IF}}+B)} = \frac{3\times10^8}{2\times(5.115\times10^6+1.023\times10^6)} \approx 25$ m for f_{IF_1} and f_{IF_2} respectively. The verdict will be verified by the result with respect to range compressed pulse and the corresponding point spread function [11] shown in Figure 4.

From Figure 4, we can see that based on a standard GPS C/A code signal receiver, the range compressed pulse based on the proposed algorithm is around 3 times thinner and 6 times thinner than the conventional algorithm with f_{IF_1} and f_{IF_2}, respectively.

To verify the proposed range compression algorithm, a simulation test is carried out. The simulation experiment is set out as shown in Figure 5.

In Figure 5, four strong reflection surfaces with 400 m long and 20 m width are arranged with 200 m along the azimuth direction and 108 m with the range direction. The direct and reflect signal antennae are moving along the azimuth direction with a constant speed to perform aperture synthetic. The GPS data are simulated using parameters listed in Table 1. Based on the considered scenarios, the GNSS-SAR images generated by both the proposed range compression scheme and the conventional range compression scheme are shown in Figure 6.

As can be seen in Figure 6(a) and (b), due to the fact that the proposed scheme can offer a superior range resolution, the four scattering areas in Figure 5 can be well separated. Through the comparisons, Figure 6(b) has a less range ambiguity because a higher IF value is employed at the GPS receiver. In Figure 6(c), the two scatters located at different range domain cannot be separated on the GNSS-SAR image with the conventional range compression algorithms as the resolution of this approach is 150 m according to (17) with $B = 1.023$ MHz.

In summary, the simulation results in this section has demonstrated that the proposed range compression algorithm can provide a superior range resolution than the conventional range compression algorithm.

Furthermore through tests, the proposed range compression algorithm is also applicable for the GNSS-SAR receiver based on the other GNSS signals of opportunity. Since for most GNSS signals receiver, the IF values are typically higher than the baseband frequency (which equals to PRN code chip rate), a superior range resolution should be achieved by employing the proposed algorithm. However because GNSS receivers differ in the PRN code types and IF values for signals receiving, the achievable range resolutions after improving will be different.

5. Discussion

Although the proposed algorithm can significantly improve range resolution of GNSS-SAR, according to Figure 4 to Figure 6, it can be seen that the magnitude decreases with respect to f_{IF} values. This is because when performing spectrum equalization, Signal-to-Noise Ratio (SNR) will decrease with respect to the selected cutoff frequency [11].

Meanwhile due to the fact that spectrum equalization is employed, range compressed delay of the proposed algorithm is supposed to be higher than convention range compression algorithm. According to machine running time, range compressed delay per azimuth bin with respect to the two algorithms is given as Table 2.

Table 2. The average range compressed delay per azimuth bin

The conventional range compression algorithm	The proposed range compression algorithm with $f_{\mathrm{IF}_1} = 2.092$MHz	The proposed range compression algorithm with $f_{\mathrm{IF}_2} = 5.115$MHz
0.00425 s	0.13308 s	0.16558 s

Preprints (www.preprints.org) | NOT PEER-REVIEWED | Posted: 23 March 2017 doi:10.20944/preprints201703.0179.v1

Peer-reviewed version available at Sensors 2017, 17, 1496; doi:10.3390/s17071496

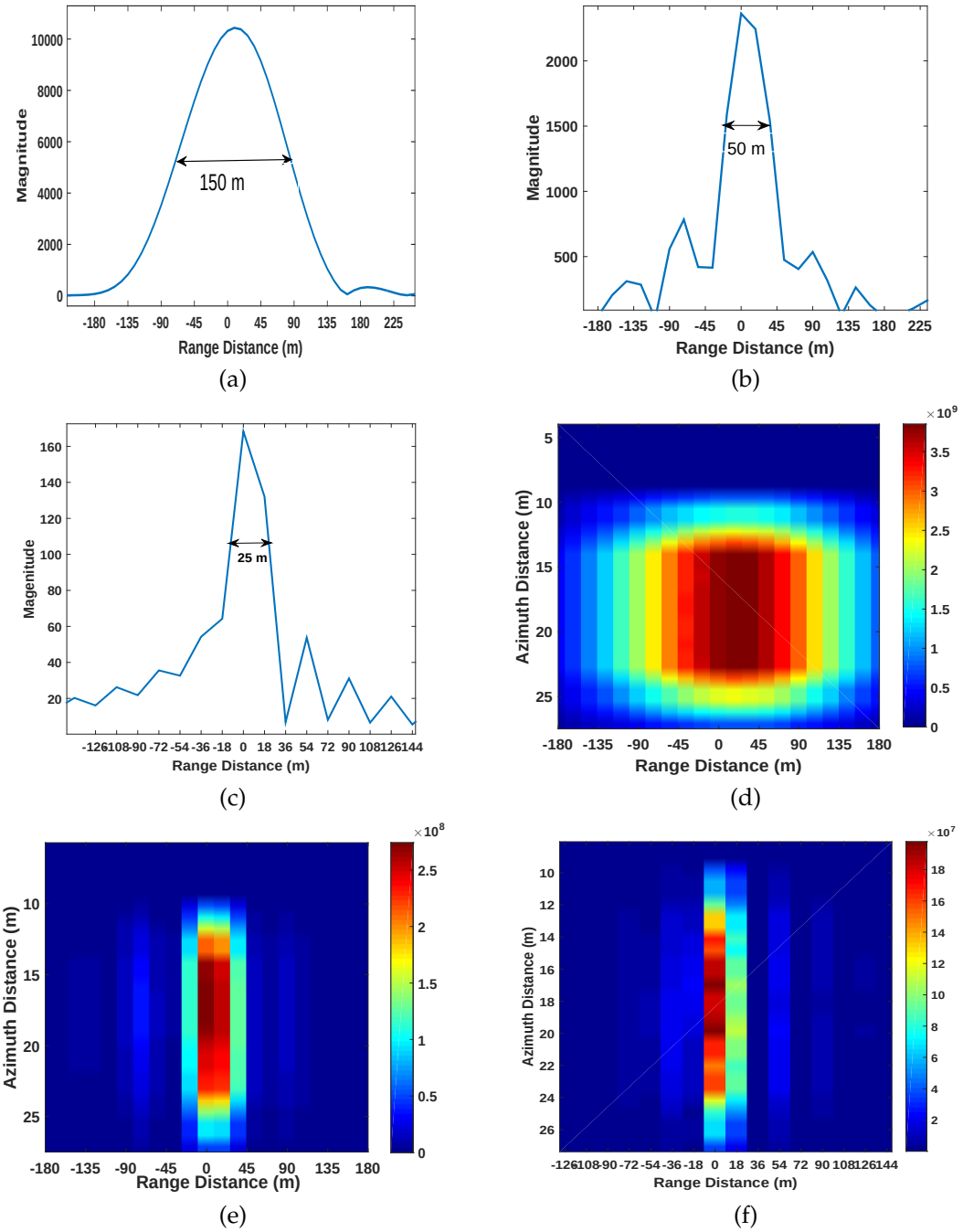

Figure 4. (a) Range compressed pulse based on the conventional range compression algorithm; (b) Range compressed pulse based on the proposed range compression algorithm with $f_{\mathrm{IF}_1} = 2.092\mathrm{MHz}$; (c) Range compressed pulse based on the proposed range compression algorithm with $f_{\mathrm{IF}_2} = 5.115\mathrm{MHz}$; (d) The point spread function of (a); (e) The point spread function of (b); (f) The point spread function of (c).

Preprints (www.preprints.org) | NOT PEER-REVIEWED | Posted: 23 March 2017 doi:10.20944/preprints201703.0179.v1

Peer-reviewed version available at Sensors 2017, 17, 1496; doi:10.3390/s17071496

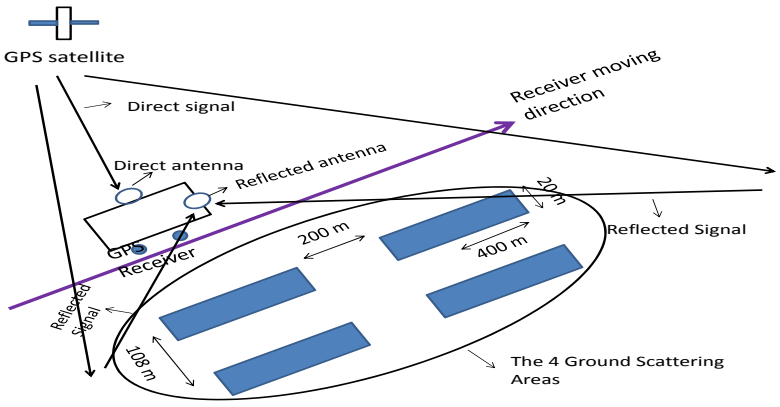

Figure 5. The simulation scenario.

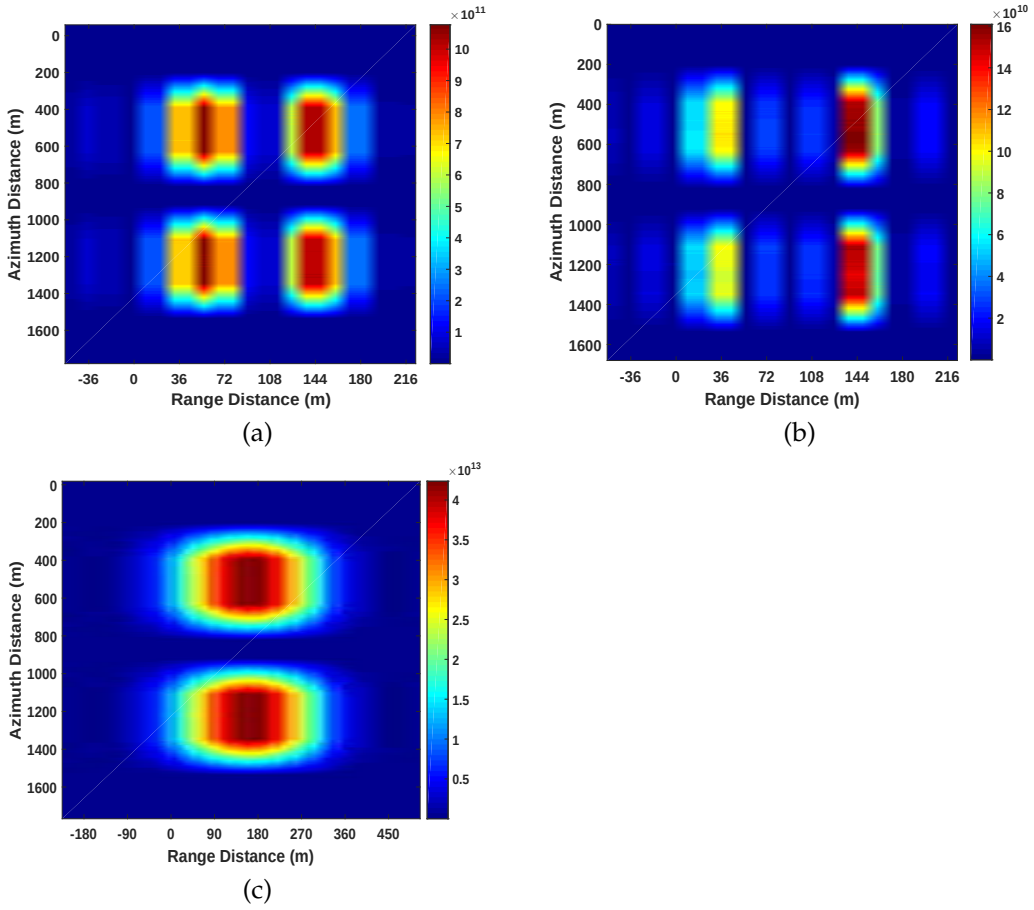

Figure 6. (a) GNSS-SAR image generated by the proposed range compression algorithm with f_{IF_1} = 2.092MHz; (b) GNSS-SAR image generated by the proposed range compression algorithm with f_{IF_2} = 5.115MHz; (c) GNSS-SAR image generated by the conventional range compression algorithm.

As we can see that in Table 2, range compressed delay increases with respect to IF value as well.

Therefore in our future work, we would like to develop a mechanism for selecting the optimal IF value for GNSS-SAR receivers to trade-off among range resolution, range compressed SNR and compressed delay together with corresponding field experimental studies.

6. Conclusions

In this paper, a novel range compression algorithm for enhancing the resolution of GNSS-SAR is proposed. In range compression, the received reflected IF GNSS signal is correlated with the synchronized direct baseband signal in range domain for each azimuth bin. Then side lobes of the range compressed result are suppressed by a proper designed spectrum equalization window. Both theoretical derivation and simulation results have demonstrated that the proposed range compression algorithm can provide a superior range resolution than the conventional range compression algorithm in GNSS-SAR. At the same time, the proposed algorithm can improve range resolution without the need for generating full preliminary images.

Acknowledgments: The research was substantially by funded by the grants from The National Key Research and Development Program of China (No. 2016YFB0501803).

Author Contributions: Yu Zheng proposes the idea, conducts the theoretical derivation, simulations as well as carries out writing the paper. Yang Yang helps to discuss the related technical issues. Wu Chen revises the manuscript.

Conflicts of Interest: The authors declare that there is no conflict of interests.

Abbreviations

The following abbreviations are used in this manuscript:

GNSS	Global Navigation Satellite System
GPS	Global Positioning System
SAR	Synthetic Aperture Radar
IF	Intermediate Frequency
SNR	Signal to Noise Ratio
C/A code	Coarse Acquisition Code
P code	Encrypted Precision Code
FOV	Field of Version

Bibliography

1. Zuo, R. *Bistatic synthetic aperture radar using GNSS as transmitters of opportunity*; PhD diss., University of Birmingham, 2012.
2. Zeng, Z. *Passive bistatic SAR with GNSS transmitter and a stationary receiver*; PhD diss., University of Birmingham, 2013.
3. Daout, F.; Schmitt, F.; Ginolhac, G.; Fargette, P. Multistatic and multiple frequency imaging resolution analysis-application to GPS-based multistatic radar. *IEEE Transactions on Aerospace and Electronic Systems*, 2012, 48(4), 3042–3057.
4. Mikawa, Y.; Ebinuma, T. and Nakasuka, S. The study of the remote-sensing application using the GNSS reflected signal with the aperture synthesis. *2012 IEEE International InGeoscience and Remote Sensing Symposium (IGARSS)*, 2012, 400–403.
5. Ebinuma, T.; Mikawa, Y. and Nakasuka, S. Quasi-monostatic algorithm for GNSS-SAR. *2013 IEEE Asia-Pacific Conference on InSynthetic Aperture Radar (APSAR)*, 2013, 164–166.
6. Lazarov, A.; Chen, V. C.; Kostadinov, T. and Morgado, J. P. Bistatic SAR system with GPS transmitter. *2013 IEEE InRadar Conference (RADAR)*, 2013, 1–6.
7. Antoniou, M.; Zeng, Z.; Feifeng, L. and Cherniakov, M. Experimental demonstration of passive BSAR imaging using navigation satellites and a fixed receiver. *IEEE Geoscience and Remote Sensing Letters*, 2012, 9(3), 477–481.

8. Antoniou, M.; Hong, Z.; Zhangfan, Z.; Zuo, R.; Zhang, Q. and Cherniakov, M. Passive bistatic synthetic aperture radar imaging with Galileo transmitters and a moving receiver: Experimental demonstration. *IET Radar, Sonar & Navigation*, 2013, 7(9),985–993.
9. Antoniou, M. and Cherniakov, M. GNSS-based bistatic SAR: A signal processing view. *EURASIP Journal on Advances in Signal Processing*, 2013,(1), 98.
10. Santi, F.; Pastina, D.; Bucciarelli, M.; Antoniou, M.; Tzagkas, D. and Cherniakov, M. Passive multistatic SAR with GNSS transmitters: Preliminary experimental study. *2014 IEEE 11th InEuropean Radar Conference (EuRAD)*, 2014, 129–132.
11. Ma, H.; Antoniou, M. and Cherniakov, M. Passive GNSS-Based SAR Resolution Improvement Using Joint Galileo E5 Signals. *IEEE Geoscience and Remote Sensing Letters*, 2015, 12(8), 1640–1644.
12. Ma, H.; Antoniou, M. and Cherniakov, M. Passive GNSS-based SAR imaging and opportunities using Galileo E5 signals. *Science China Information Sciences*, 2015, 58(6), 1–11.
13. Santi, F.; Antoniou, M. and Pastina, D. Point spread function analysis for GNSS-based multistatic SAR. *IEEE Geo-science and Remote Sensing Letters*, 2015, 12(2), 304–308.
14. Zeng, T.; Zhang, T.; Tian, W. and Hu, C. Space-Surface Bistatic SAR Image Enhancement Based on Repeat-Pass Coherent Fusion With Beidou-2/Compass-2 as Illuminators. *IEEE Geoscience and Remote Sensing Letters*, 2016, 13(12), 1832–1836.
15. Zeng, H., et al. A Novel General Imaging Formation Algorithm for GNSS-Based Bistatic SAR.*Sensors*, 2016, 16(3), 294.
16. Santi, F.; Bucciarelli, M., Pastina, D.; Antoniou, M. and Cherniakov, M. Spatial resolution improvement in GNSS-Based SAR using multistatic acquisitions and feature extraction. *IEEE Transactions on Geoscience and Remote Sensing*, 2016, 54(10),6217–6231.
17. Shi, S.; Liu, J.; Li, T. and Tian, W. Basic performance of space-surface bistatic SAR using BeiDou satellites as transmitters of opportunity. *GPS Solutions*, 2016, 1–11.
18. Lv, G.; Wang, J. and Liu, X. Ground moving target indication in SAR images by symmetric defocusing. *IEEE Geoscience and Remote Sensing Letters*, 2013, 10(2), 241–245.
19. Walterscheid, I.; Espeter, T.; Brenner, A. R.; Klare, J.; Ender, J. H.; Nies, H.; Wang, R. and Loffeld, O. Bistatic SAR experiments with PAMIR and TerraSAR-X—setup, processing, and image results. *IEEE Transactions on Geoscience and Remote Sensing*, 2010, 48(8), 3268–3279.
20. Rodriguez-Cassola, M.; Baumgartner, S.V.; Krieger, G.and Moreira, A. Bistatic TerraSR-X/F-SAR Spaceborne—Airborne SAR Experiment: Description, Data Processing and Results. *IEEE Transactions on Geoscience and Remote Sensing*, 2010, 48(2), 781—794.
21. Sklar, B. *Digital communications*, NJ: Prentice Hall, Jan. 1, 2001.
22. Sukhatme, B. V. *Sampling theory of surveys with applications*, 1954.